



Dissimilar joining of stainless steel and aluminum using twin-wire CMT

Wanghui Xu^{1,2} · Huan He³ · Yaoyong Yi¹ · Haiyan Wang¹ · Chen Yu¹ · Weiping Fang¹

Received: 9 September 2020 / Accepted: 31 January 2021 / Published online: 23 February 2021
© International Institute of Welding 2021

Abstract

The twin-wire CMT with Al-Si filler was used as weld/brazing process for dissimilar joining of stainless steel and aluminum. It is shown that this approach can ensure a satisfactory performance of the joint and the dissimilar joint exhibits typical characteristics of common known steel/aluminum weld brazing joints. Intermetallic compounds (IMCs) were detected next to the steel as a layer of Fe_2Al_5 , as a layer of $\text{Fe}_3\text{Al}_2\text{Si}_4$ adjacent to the aluminum side and as a scattered phase of $\text{Fe}_4\text{Al}_{13}$ in between. The total thickness of the IMCs was determined with 2–4 μm . The maximum tensile strength of the weld joints without reinforcement was up to 96 MPa and cross tensile test specimens fractured at the brazing interface at about 35% of the strength of the aluminum. An increase of the wire feeding rate and decrease of the welding speed thereby outperform beneficial in respect to wetting characteristics. However, excessive heat input (e.g., wire feeding rate larger than 7.5 m/min) causes a reduction of the mechanical properties. A groove gap about 1 mm ensures furthermore a good back appearance.

Keywords Twin-wire CMT · Weld brazing · Stainless steel/aluminum alloy · Welding formation · Metallography

1 Introduction

Dissimilar joining of aluminum and stainless steel has been widely applied in aerospace, transportation, and other fields. As a consequence, joining of aluminum alloys to stainless steel has become a hot research field, and this raised higher requirements for the joining process and joint performance [1]. However, aluminum and steel are not suitable for fusion welding due to the large difference in their melting points (660 °C for Al and 1538 °C for Fe), the nearly zero solid solubility of iron in aluminum, and the formation of brittle intermetallic

compound (IMC, as e.g. Fe_2Al_5 and FeAl_3), over a wide range in the Fe-Al-constitution diagram [2]. If these IMCs exceed a critical thickness, the joint is prone to crack under very small stresses, resulting in a sharp decline in mechanical properties of the joint [3]. That is why the control of the formation of Fe-Al IMCs is the most challenging topic in joining of stainless steel and aluminum.

In order to achieve the reliable stainless steel/aluminum dissimilar joint, several solid state welding methods were employed to control the growth of intermetallic compounds, such as diffusion welding, brazing, friction welding [4], and friction stir welding [5]. But these methods have some disadvantages, such as limited dimension, high loading requirement, and complex process.

But these methods are very complex, are limited in the dimension of the joint, or require high process forces. Previous research indicated that arc weld brazing is a promising welding technique which is capable to obtain joints of Al/Fe with acceptable properties [6] [7] [8].

Song et al. used the TIG weld brazing process with a modified non-corrosive flux to join dissimilar metals of 5A06 aluminum alloy and SUS 321 stainless steel [9]. The results showed that the stainless steel and aluminum alloy could be joined successfully and the IMC layer is 3–5 μm (less than the limited value of 10 μm) [9]. But the formation stability and

Recommended for publication by Commission II - Arc Welding and Filler Metals

✉ Wanghui Xu
xuwanghui@126.com

¹ Guangdong Provincial Key Laboratory of Advanced Welding Technology, Guangdong Welding Institute (China-Ukraine E.O.Paton Institute of Welding), No.363, Changxing Road, Tianhe District, Guangzhou 510650, People's Republic of China

² State Key Laboratory of Advanced Welding and Joining, Harbin Institute of Technology, Harbin, People's Republic of China

³ School of Nuclear Equipment and Nuclear Engineering, Yantai University, Yantai, People's Republic of China

Table 1 Chemical composition of the base and filler metal (wt%)

Chemical elements	Mg	Si	Cu	Zn	Mn	Ti	Cr	Fe	C	S	P	Mo	Ni	Al
Aluminum	≤ 4.5	≤ 0.20	0.01	0.15	0.80	0.80	0.09	0.10	-	-	-	-	-	Bal.
Steel	-	≤ 1.00	-	-	≤ 2.0	-	18–20	Bal.	≤ 0.08	≤ 0.030	≤ 0.025	0.30	8–11	-
Filler metal	≤ 0.10	5	≤ 0.05	-	-	-	0.80	0.03	-	-	-	-	-	Bal.

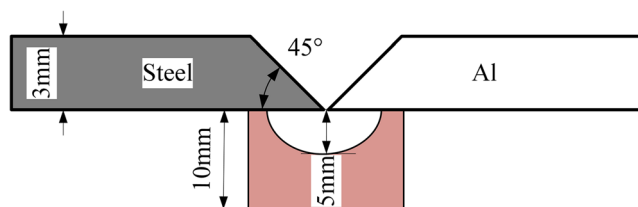
mechanical properties of the joint should be further improved. In order to control the heat input and improve the welding stability, a TIG weld brazing process with twin hot wires was employed to joining aluminum alloy and stainless steel [10] [11]. By employing the twin hot wires, the welding current is reduced, the thickness of the IMC layer decreased, and the tension strength improved. Shao et al. investigated the interfacial microstructures of aluminum and galvanized steel dissimilar joint obtained by pulsed twin electrode gas metal arc weld brazing [12]. The results showed that the twin gas metal arc welding has an advantage of low heat input, which is beneficial to obtain good mechanical properties of the joint. The MIG/TIG double-sided arc weld brazing was proposed to a joint of dissimilar alloys [13] [14]. There were favorable surface and back appearance, and the highest tension strength of the joint of Al/steel can be up to 150 MPa.

The cold metal transfer (CMT) process is a new technique and becomes a hot research field in dissimilar materials welding [15, 16] due to the advantages of high efficiency and low heat input. However, the twin-wire CMT welding has more obvious advantages than traditional single-wire CMT welding for joining dissimilar metals, such as less heat input for controlling IMC, independent adjustment of fillers, and welding parameters of steel and aluminum. Therefore, this paper developed the twin-wire CMT weld brazing technology to the butt joining of 3-mm aluminum and steel plate and studied the bead formation, metallography, and joint strength.

2 Experimental materials and procedure

2.1 Materials

The materials used in this experiment were 5083 aluminum alloy and SUS304 austenitic stainless steel sheets in 3.0-mm thickness. The filler material was 4043 aluminum alloy with a

**Fig. 1** Geometry of the groove

diameter of 1.2 mm. The chemical compositions of the base and filler metals are shown in Table 1.

In this experiment, the modified Nocolock fluoride brazing flux was coated on the surface of SUS304 stainless steel. The main components of the coating layer are $KAlF_4$ and AlF_3 .

2.2 Experimental procedure

The geometry of the groove prepared for weld brazing experiment is shown in Fig. 1, the surface of which was cleaned by abrasive paper, scraper, and acetone before weld brazing. The groove of the joint was in the pattern of “V,” and the bevel angle was 45° . The Nocolock flux suspension (flux powder dissolved in acetone) was smeared homogeneously with brush in 0.2–0.5-mm thick on the groove face and both the front and back faces of the steel. The width of butt gap was 0–1 mm. There is a circular shaped groove with the depth of 5 mm and width of 10 mm in the copper backing plate of 10 mm × 10 mm in size. Twin Fronius TPS CMT power sources were employed in this research, and the schematic of twin-wire CMT welding system is shown in Fig. 2. The CMT welding process was applied in this experiment. In the CMT welding process, when the welding wire is short circuited with the molten pool, the wire can be drawn back, and the welding current can be reduced, so as to reduce the welding heat input. The wire push/pull frequency was 70 Hz in this experiment. The shielding gas used in this experiment is Ar, and the gas flow rate is 15 L/min.

After welding, one metallographic and three tensile test specimens were cut from each weld plate by super wire cutting machine, and metallographic samples were ground with grinding papers and polished by 300, 500, and 1000 SiC grades and followed by 1 μm diamond suspension to mirror-like surface aspect. Then the macrostructure of the joint was observed using optical metalloscopy after the samples were etched in Keller’s reagent about 3–5 s, for optical metallography ZEIS IMAGER was used. The microstructure and composition of interface layer were researched by Hitachi S-3400 scanning electron microscope and energy dispersive spectrometer. Transmission electron microscope (TEM) samples of about $25 \times 25 \times 0.05 \mu\text{m}^3$ were prepared from the cross-sections of the joint using a FEI Helios NanoLab 600i FIB with a Ga+ ion accelerating voltage of 30 kV. TEM was

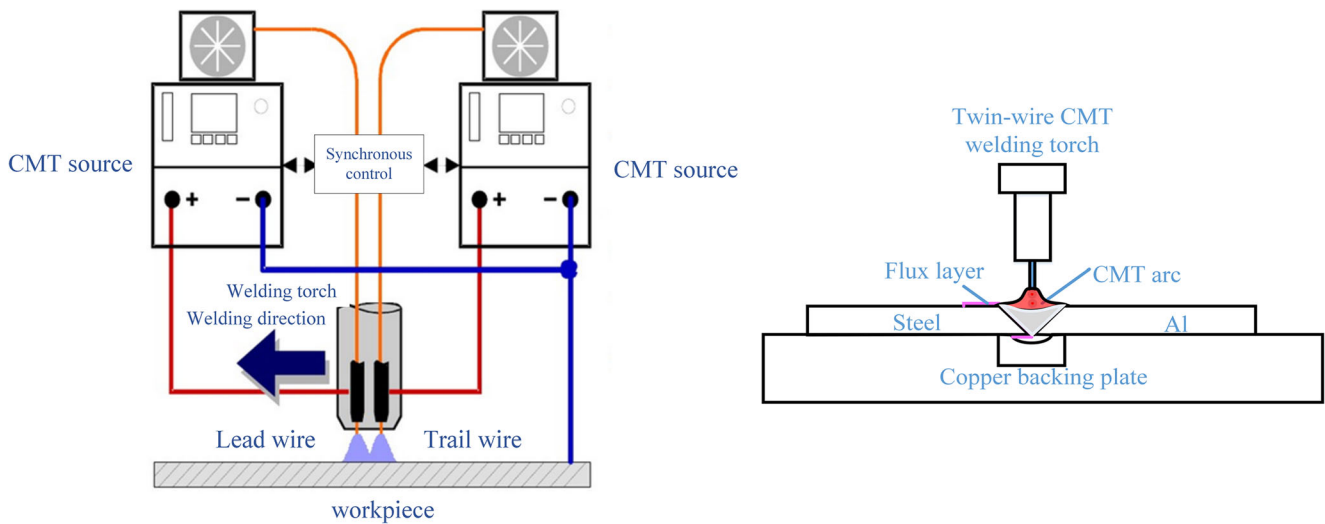


Fig. 2 Schematic illustration of twin-wire CMT welding-brazing

Table 2 Welding parameters

No	Wire feed rate (lead and trail wire) (m/min)	Welding speed (mm/min)	Butt gap (mm)	Welding current (lead and trail wire) (A)	Voltage (lead and trail wire)
1	5	400	0	80	17
2	6	400	0	90	17.5
3	7	400	0	100	18.2
4	7.5	400	0	105	18.8
5	6	400	1	90	17.5
6	6	600	1	90	17.5
7	6	700	1	90	17.5
8	6	800	1	90	17.5

performed using a FEI Titan G2 60-300 operating at 300 kV for bright-field (BF) imaging and scanning transmission electron microscopy (STEM) imaging, selected area electron diffraction (SAD), and energy dispersive spectrometer (EDS)

chemical analysis. SAD patterns were indexed with the aid of the software package Digital Micrograph (version 3.7.4) and the Powder Diffraction File PDF-2 (release 2004) published by ICDD. In order to avoid the influence of weld

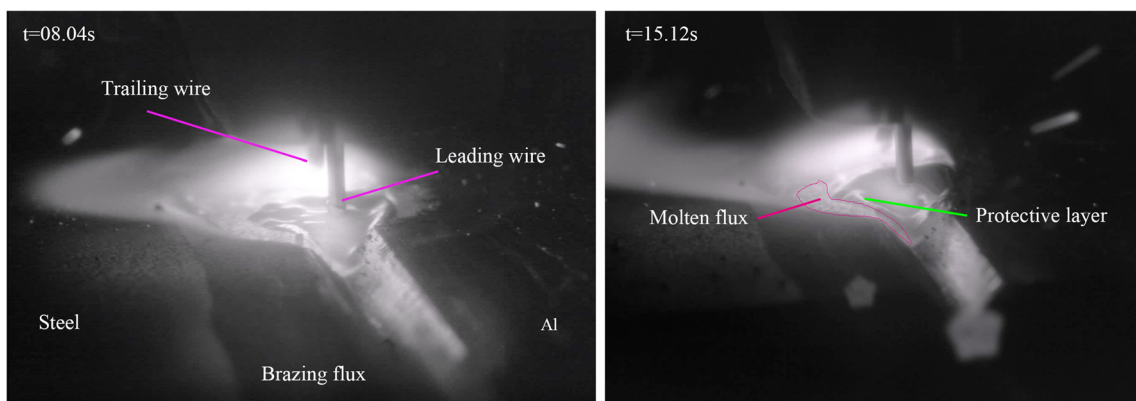


Fig. 3 Photo of twin-wire CMT weld brazing

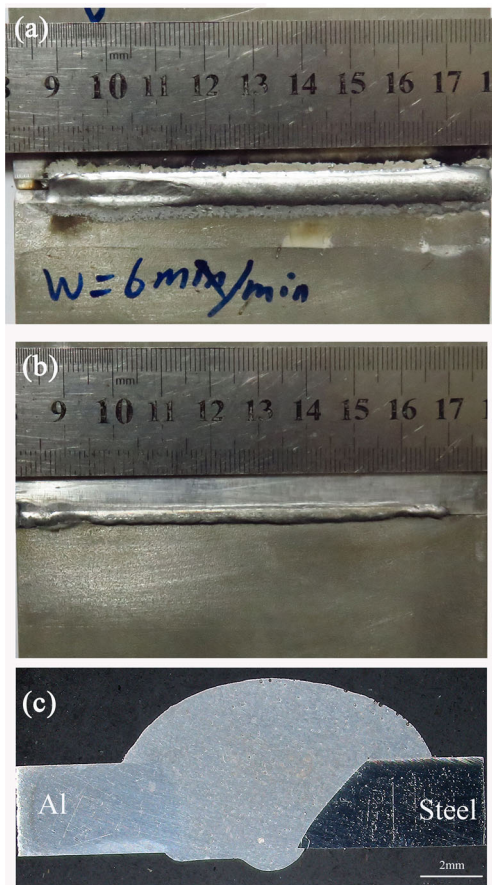


Fig. 4 Formation of twin-wire CMT weld brazing bead (welding speed: 400 mm/min): a surface appearance, b back appearance, c cross section

reinforcement on tensile test result, the reinforcement was removed from the tensile specimens.

3 Results and discussion

3.1 Filling and formation process of twin-wire CMT

The feasibility research results show that it can be obtained a joint of aluminum and steel with a wire feed rate between 5 and 8 m/min, and a welding speed between 400 and 800 mm/min. Table 2 lists the parameters used in this experiment in order to study the influences of wire feed rate, welding speed, and butt gap on formation of the joint.

Figure 3 shows the welding process of twin-wire CMT. The lead arc heats the steel side and melts the aluminum base metal. The droplet of lead wire and molten aluminum metal forms the melt pool, but it is not enough to fill the groove. Therefore, the molten metal forms a concave shape under the action of arc pressure and droplet impact force of lead wire and spreads on the groove surface. In addition, the lead arc melts the flux, and the liquid metal spreads to inner surface and upper surface of the steel groove by the help of the molten flux. There is a protective film of aluminum on the interface between steel and molten aluminum.

Then, the trail arc was generated between the trail wire end and surface of molten pool formed by the lead arc. Molten droplets of trail wire transfer to the surface of protective aluminum layer and fill the entire groove. It can be seen from Fig. 3 that the twin CMT arcs and molten filler metal deflect to the side of SUS304 stainless steel due to the effect of the Nocolock fluoride brazing flux.

In a word, the lead wire plays a major role in the melting of aluminum side and the interface reaction between steel and aluminum, while the trail wire fills the molten pool, and its arc pressure and droplet impact force increase the stirring effect of the molten pool.

3.2 Effects of welding parameters on formation

The surface appearance, back appearance, and cross section of the dissimilar metal joint are shown in Fig. 4. It presents favorable surface appearance and back appearance owing to the heat of CMT arc and the help of the flux layer. During the weld brazing process, the stainless steel is not melted because of its high melting point. The aluminum alloy filler metal is heated and melted under the heat of the arc and then spreads to the surface of stainless steel to form a good brazing joint, while the aluminum alloy base material with low melting temperatures was fusion welding joint. Therefore, the joint exhibits typical characteristics of weld brazing.

The cross sections of weld bead with different wire feed rates are shown in Fig. 5. The weld width and spread angle increase (spread angle = 180° , wetting angle) with wire feed rate (welding current) increasing, as shown in Fig. 6. The increasing of wire feed rate causes the increase of heat input and liquid metal volume, which results in the increasing of weld width and extension of weld time. The increasing of wire



Fig. 5 Macrographs of the seam with the different wire feed rate (welding speed: 400 mm/min): a 5/min, b 7 m/min, c 7.5 m/min

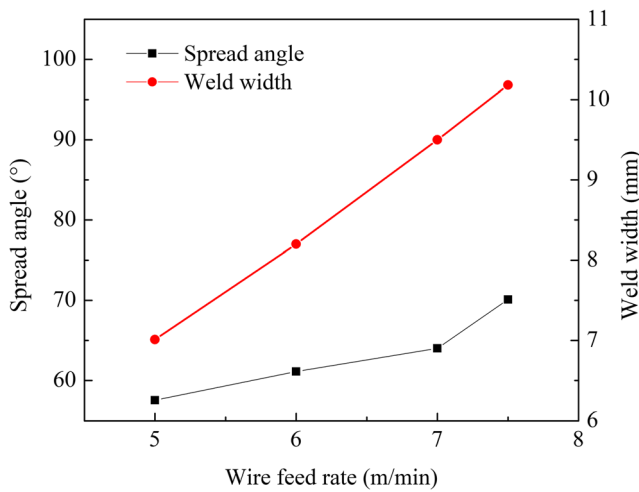


Fig. 6 Affection of wire feeding rate on weld width and spread angle

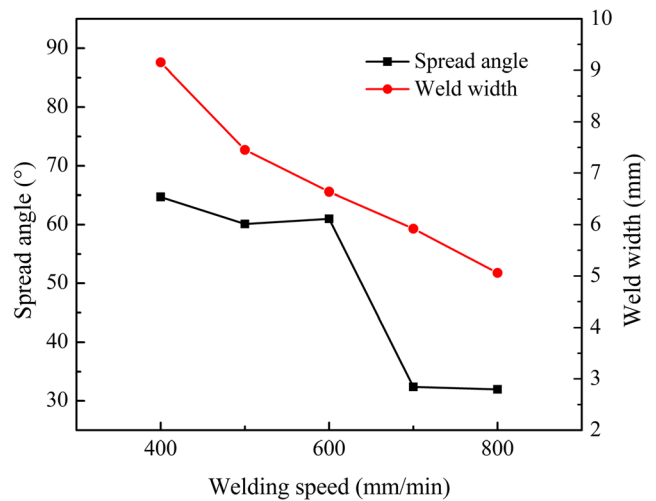


Fig. 8 Effect of welding speed on weld width and spread angle

feeding speed is also beneficial to weld back appearance and the spreading of liquid filler material to the steel side.

Figure 7 shows the cross sections of the joints with different welding speeds. The favorable surface and back appearance are obtained with the welding speed from 400 to 800 mm/min. When the welding speed is higher than 800 mm/min, the undercut defect appeared on the steel side due to a lack of liquid filler metal. The weld width and spread angle decline as the increasing of welding speed, owing to the reduction of liquid filler metal volume of per unite length. As shown in Fig. 8, the weld width and spread angle decrease with the increasing of welding speed, which is related to the decrease of heat input.

The butt gap affects the back forming of the weld, as shown in Fig. 9. When the butt gap is zero, the back forming is not uniform because the molten filler metal cannot flow to the back of the steel plate. While the butt gap is set as 1 mm, the molten filler metal wets and spreads to the back of the steel

plate. The weld bead has the favorable surface and back appearance with the gap of 1 mm.

3.3 Microstructure of weld brazing joint

Optical micrographs of fusion zone, weld metal, and the IMC layer are shown in Fig. 10. The aluminum alloy with low melting temperature was fused and mixed with the liquid filler metal to produce the welded seam with obvious fusion zone. The grain size of HAZ is larger than that of base metal. Weld metal is columnar crystals, and the strengthening phase Mg_2Si is precipitated. The IMC at the interface is a serrated structure with a thickness of about 2–5 μm , and there are a number of IMCs in the weld near the interface. It is considered that the flux layer melts rapidly under the heat action of the arc causing the filler metal wet to the stainless steel surface, and the IMC is formed at the interface between the liquid filler metal and the steel plate. The periodic push/pull welding wires will enhance

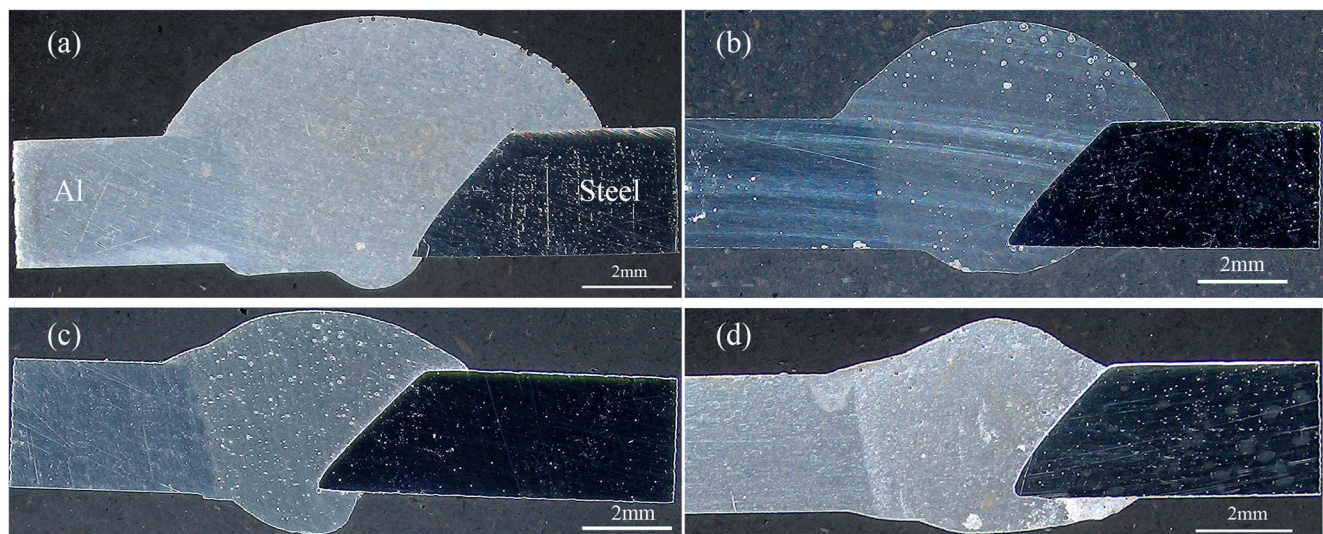
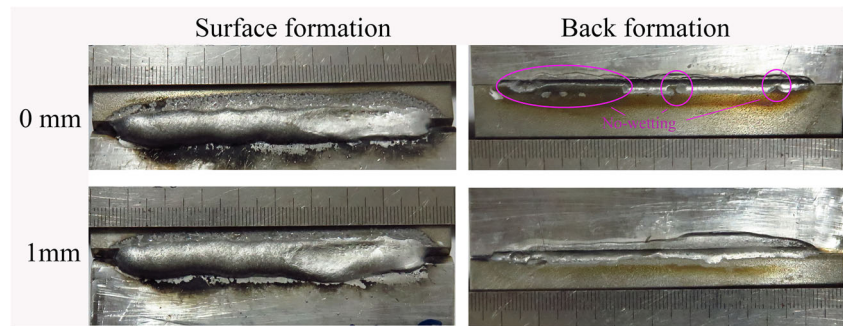


Fig. 7 Macrographs of the seam with the different welding speeds: a 400 mm/min, b 600 mm/min, c 700 mm/min, d 800 mm/min

Fig. 9 Joints with the butt gap of 0 and 1 mm



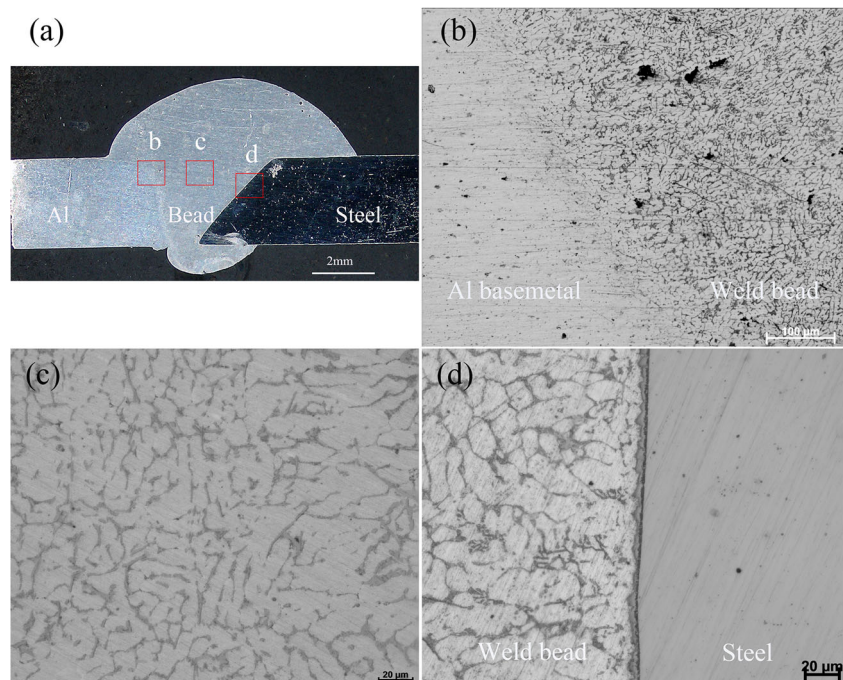
the flow of molten pool, which disrupt the direction of the growth of IMC and break some of the large serrated intermetallic compounds into the weld. The serrated IMC grow along with the direction perpendicular to the interface. There is aluminum alloy with good plasticity in the zone between two higher parts of IMC; such a jagged structure is beneficial to prevent crack propagation and play a role of “pinning” for improving the bonding strength.

The SEM was employed to observe the form of IMC in different position. As shown in Fig. 11, the average IMC thicknesses of the upper, middle, and lower areas are 3.4 μm , 4.0 μm , and 2.8 μm , respectively. The interface thickness in the middle is thicker than that in the upper and lower area, while the bottom interfacial layer is the thinnest among them. The distribution of IMC in the middle area of the interface is more uniform than that in the upper and lower area. The arc generated by the lead wire heats the stainless steel, and the aluminum solder of the lead wire reacts with the stainless steel to form a thin upper interface layer; then the trail wire arc heats

the film layer and fills the aluminum solder to form the final upper interface layer. The final upper interface layer is affected by the lead and trail arcs. In addition, because the upper area is closer to the end of the wire, the arc force is stronger, and the disturbance of the molten pool is very strong, which interrupts the growth of the interface layer. Therefore, the upper interfacial layer has thin thickness and poor uniformity. Because of the high thermal conductivity of copper backing plate, the high temperature residence time in the weld bead back is so short that the diffusion of iron is insufficient, which limit the growth of IMC and form a thin and uneven shape in the lower area.

To identify the phase structures of the IMC layers between the welded seam and stainless steel, EDS line scan and map scan of the IMC layer were carried out, respectively, as plotted in Figs. 12 and 13. It can be inferred from EDS line scan results in Fig. 12 that the interface layer formed by filling metal and steel base metal contains two phases layer. There are a α phase layer (lower Si content, high Fe content)

Fig. 10 Optical microstructures of the joint: **a** dissimilar metal joint, **b** fusion joint of aluminum, **c** weld bead, **d** interface of steel and aluminum



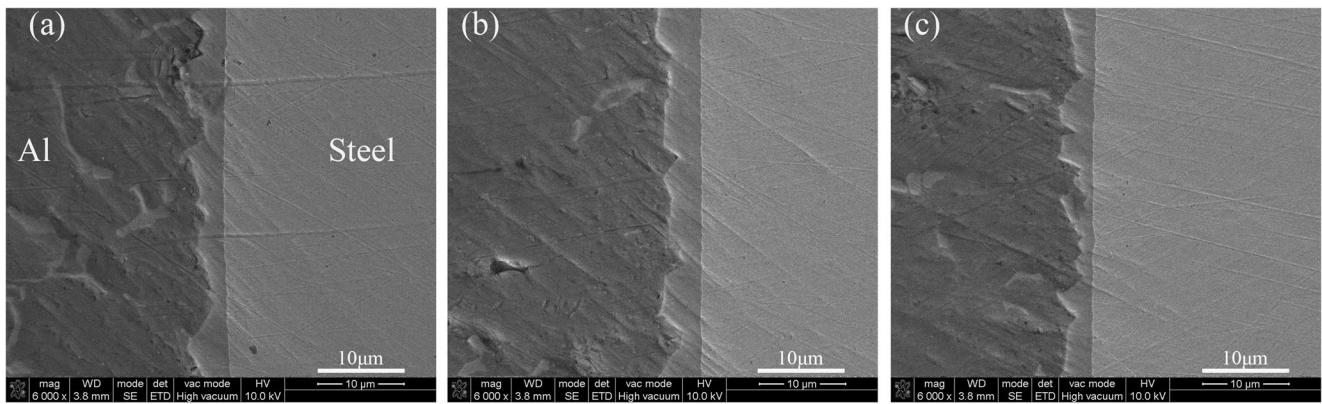
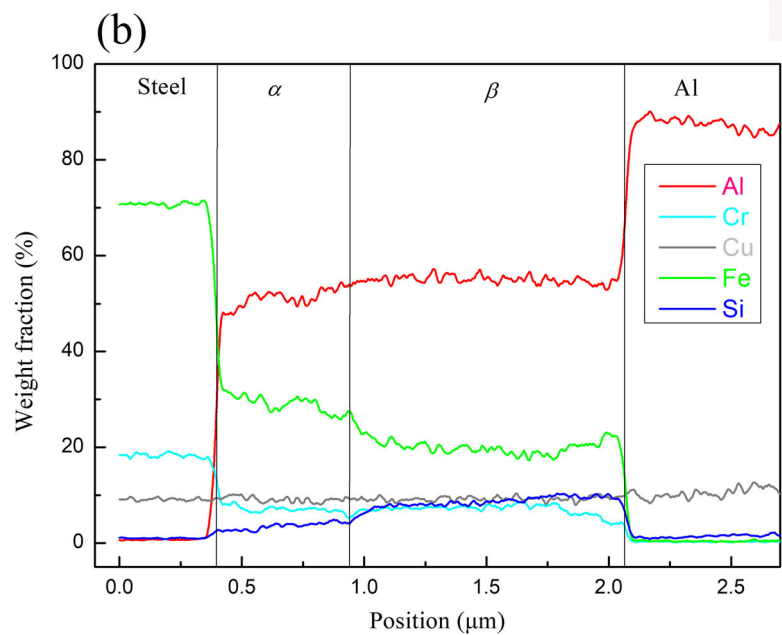
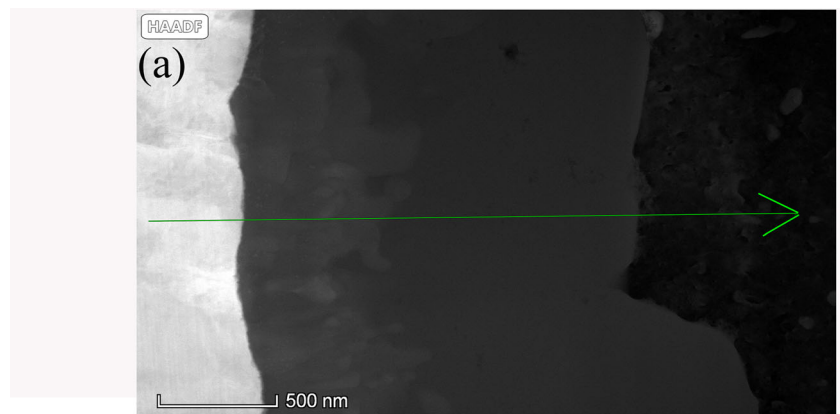


Fig. 11 SEM microstructures of interfacial layer of welded seam/stainless steel: **a** upper area, **b** middle area, **c** lower area

adjacent to the steel base metal and a β phase layer (higher Si content, lower Fe content) adjacent to the Al bead, depending on the silicon content. The EDS map scan results show that the whole interface layer consists of α and β phases. Phase α is close to the steel side, and its silicon content is lower, while Fe

content is higher. Phase β is close to the aluminum side, and its silicon content is higher, while its iron content is lower. Cr element diffuses from the stainless steel side to the aluminum weld, and the content in the interface layer is basically constant, which is about 8% in the α and β regions. After

Fig. 12 Results of EDS line scan in the interfacial layer of welded seam/stainless steel: **a** EDS line scan direction, **b** results of EDS line scan



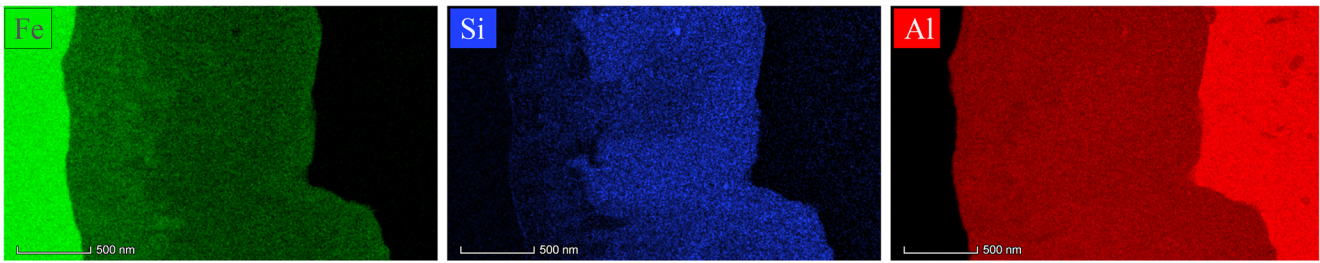


Fig. 13 Results of EDS map scan (Fe, Si, Al) in the interfacial layer

reaching the aluminum weld area, the Cr content gradually decreases and finally approaches 0. It is considered that Cr can replace part of Fe to form Fe (Cr)-Al compound [17].

It should be noted that the distribution of Cu in Fig. 12 is due to the background signal caused by the Cu grid of FIB. The samples were processed by FIB for line scanning, and FIB samples were welded on the Cu grid. In the process of EDS detection, the grid would be excited by the electron beam in different degrees and collected by the EDS probe, which eventually led to the constant content of copper distribution. This phenomenon is normal in FIB samples.

To confirm the EDS scan results and obtain phase composition of interface layer, TEM samples were prepared from localized regions of the reaction layer using FIB. A

typical STEM micrograph and corresponding SAED patterns taken at interface layer of the weld bead and steel are shown in Fig. 14. The TEM micrographs show that the interface layer is mainly composed of two phases: α phase near the steel side and β phase near the aluminum side, while a small amount of σ phase is scattered among α phase. By means of SAED, it is determined that the α phase is Fe_2Al_5 , the β phase is $\text{Fe}_3\text{Al}_2\text{Si}_4$, and the σ phase scattered between the α phases is $\text{Fe}_4\text{Al}_{13}$. Since the filler metal is Al-Si material, the content of silicon in the zone near the Al side is higher, resulting in the formation of $\text{Fe}_3\text{Al}_2\text{Si}_4$. While the diffusion of silicon near the steel side is less, so the dominant phase is Fe_2Al_5 . The TEM results are in agreement with those of EDS scan results.

Fig. 14 TEM analysis of the interfacial region between steel and aluminum weld seam

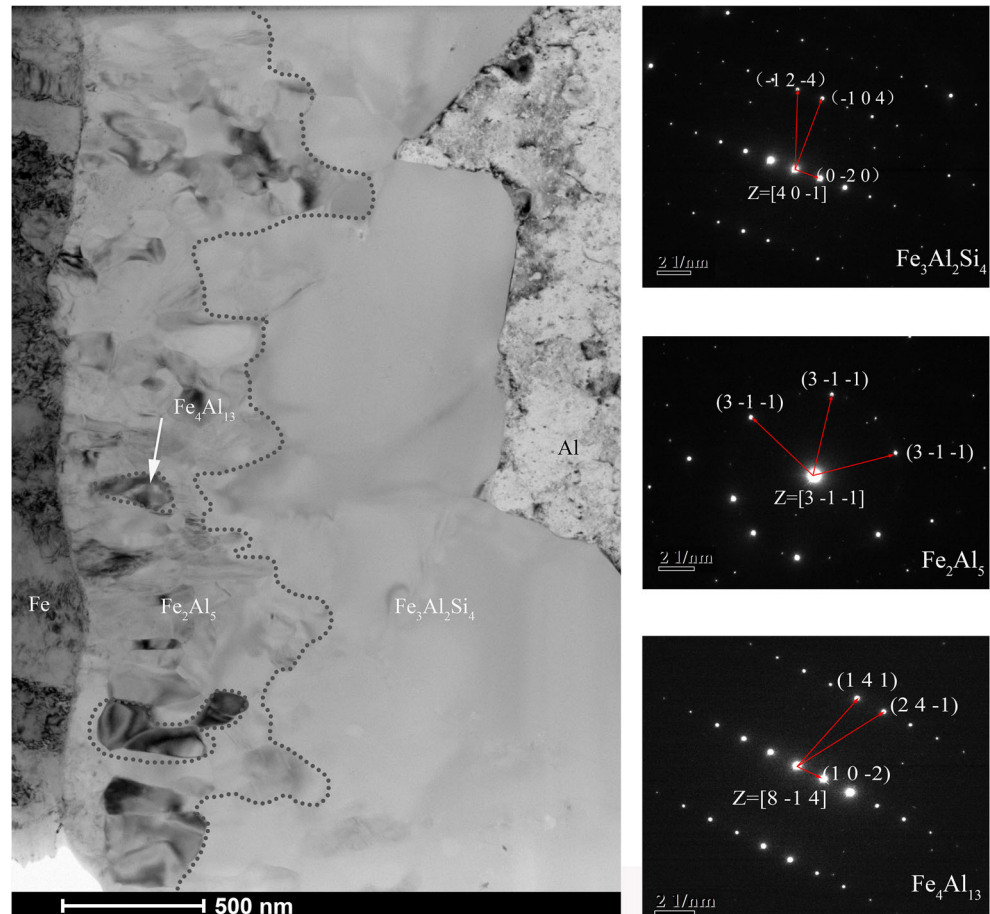


Table 3 Results of tensile test (skip strength)

No.	Tensile strength (MPa)	Fracture position
1	77	IMC
2	70	IMC
3	81	IMC
4	62	IMC
5	92	IMC
6	95	IMC
7	96	IMC
8	88	IMC

3.4 Mechanical properties

The transverse tensile properties of the twin-wire weld brazing joint of aluminum alloy and stainless steel are evaluated in this paper. Three test samples were prepared in each joint, and the results are shown in Table 3. The maximum tensile strength of the joints is up to 96 MPa, while the tensile strength of 5083 aluminum is 270 MPa. During the tensile tests, all the specimens were found to fracture along the interface of IMC, as shown in Fig. 15, and the fracture exhibited typical brittle features. The welding parameters have little effect on the strength of the joint owing to the removal of weld reinforcement. However, excessive heat input (e.g., wire feeding rate larger than 7.5 m/min) will cause the reduction of mechanical property.

3.5 Reaction mechanism of IMC layers

In twin-wire CMT weld brazing of aluminum and stainless steel, IMC layers are formed at the interface between the melted aluminum filler material and the solid stainless steel base material. The Gibbs free energies of Fe_2Al_5 and FeAl_3 ($\text{Fe}_4\text{Al}_{13}$ is sider- FeAl_3) at 1000 °C, 450 °C, and 20 °C were calculated in literature [12]. The results show that Gibbs free energies of Fe_2Al_5 are less than FeAl_3 at 1000 °C, and FeAl_3 is less than Fe_2Al_5 at 20 °C, so it can be inferred that Fe_2Al_5 takes precedence over FeAl_3 or $\text{Fe}_4\text{Al}_{13}$ during cooling. Phase

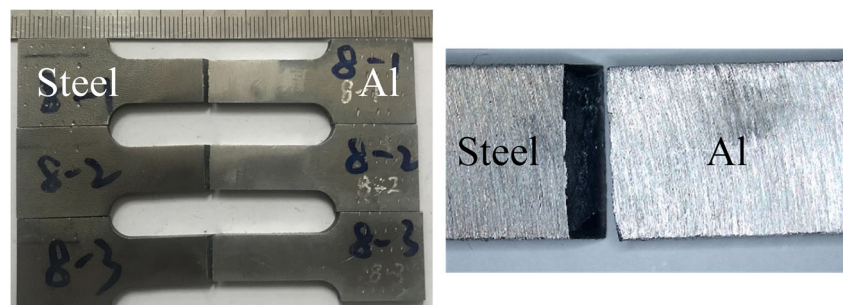
diagrams in the Fe-Al system are calculated in document [18]. The results show that the crystallization temperature of Fe_2Al_5 is higher than that of $\text{Fe}_4\text{Al}_{13}$. Consistent with previous conclusions, Fe_2Al_5 takes precedence over $\text{Fe}_4\text{Al}_{13}$ in the cooling process.

According to the results of references, it can be inferred that the interfacial reaction process in this experiment is as follows. The iron element in the solid base metal diffuses into the liquid molten pool and reacts with Al preferentially to form Fe_2Al_5 for the heating of the front arc. Due to the short reaction time, some $\text{Fe}_4\text{Al}_{13}$ phases are also formed in the non-equilibrium reaction, which takes the form that part of $\text{Fe}_4\text{Al}_{13}$ phases are distributed in Fe_2Al_5 . The welding wire contains 5% Si. The addition of silicon element in the aluminum filler wire makes the phase composition of IMC layers change remarkably. With the accumulation of Si in the interface layer, the Fe-Al-Si system is formed. And the $\text{Fe}_3\text{Al}_2\text{Si}_4$ is the Fe-Al-Si system reactant, which is consistent with reference [19].

Figure 16 shows the reaction process of the interface layer. The interface reaction process is as follows: With the diffusion of Fe and Al, the Fe_2Al_5 layer is formed at the steel side of the interface first, then the temperature of the molten pool decreases, some $\text{Fe}_4\text{Al}_{13}$ blocks precipitate in the Fe_2Al_5 layer, and the $\text{Fe}_3\text{Al}_2\text{Si}_4$ layer is formed by Si academician near the Al side. Cr in stainless steel diffuses into the interface layer and weld joint to replace some Fe atoms, which will form compounds with Al and Si, and a small amount of Cr-Al-Si compounds will be formed near the stainless steel side.

The distribution of IMC layers is also influenced by the tandem arrangement of the welding wire or arc. The protective layer formed by the lead wire and the steel base metal reduces the diffusion rate of Fe and increases the difficulty of the diffusion of Fe into the liquid molten pool formed by the trail wire. Therefore, the main function of the trail wire or arc is to fill the weld. The thickness of IMC layer in twin-wire CMT weld brazing is thinner than that in literature [12, 20]. The reason is that the lead wire produces IMC

Fig. 15 Fracture position of tensile test specimen



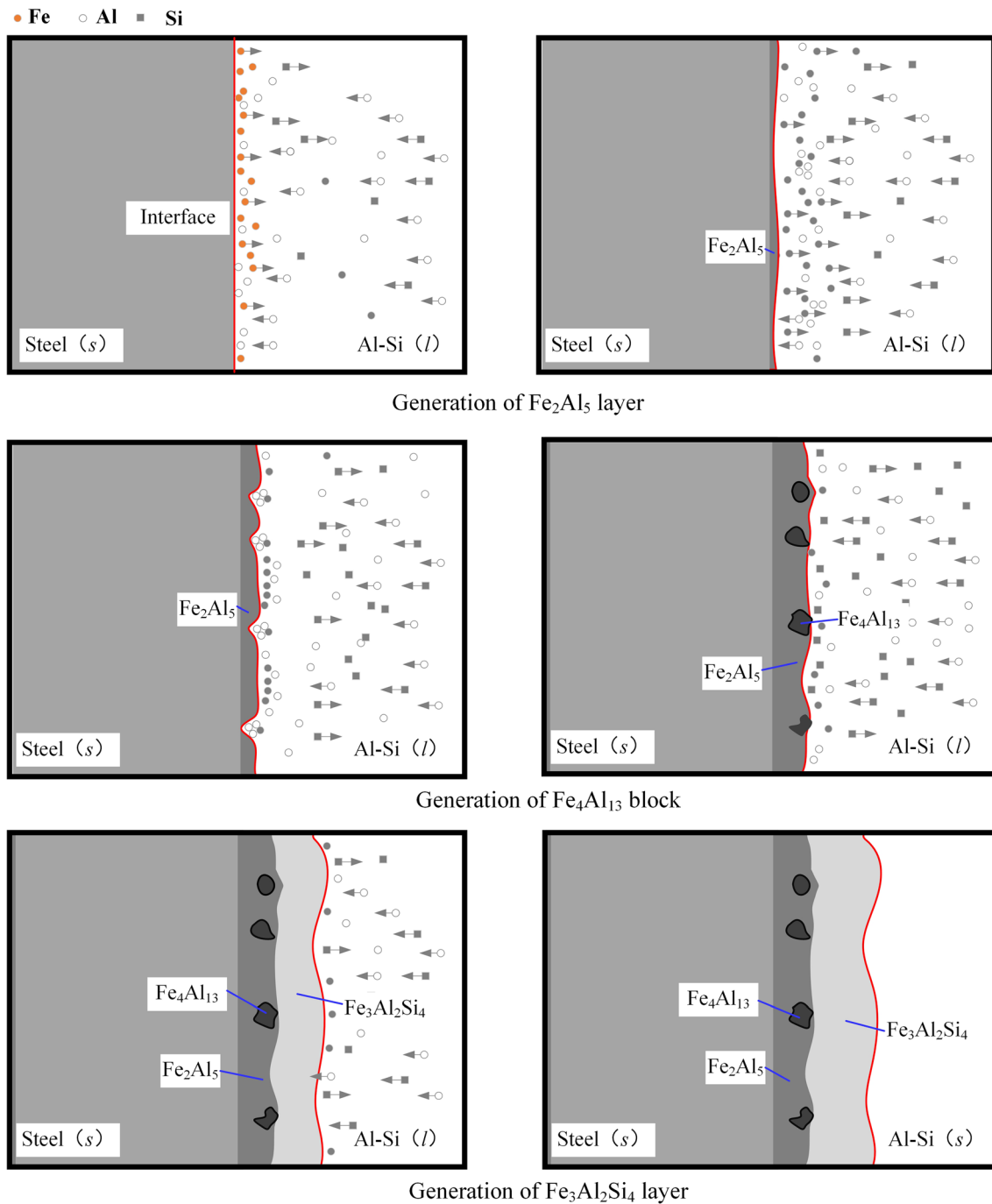


Fig. 16 Reaction process of the interface layer

protective layer with lower heat input, which hinders the further rapid growth of metal compounds.

4 Conclusions

(1) A butt weld brazing joint of 5083 aluminum alloy and SUS304 austenite stainless steel sheets in 3.0-mm

thickness was achieved by the twin-wire CMT weld brazing technique.

(2) The joint of aluminum alloy to stainless steel exhibits typical characteristics of weld brazing. The IMCs have a total thickness of 2–4 μm and present serrated structures. The EDS scan and TEM results show that the IMC interface is composed of Fe₂Al₅, Fe₃Al₂Si₄, and Fe₄Al₁₃ phases. The phase near the steel side is

Fe_2Al_5 , and $\text{Fe}_3\text{Al}_2\text{Si}_4$ is near the aluminum side, while a small amount of $\text{Fe}_4\text{Al}_{13}$ is scattered among the Fe_2Al_5 phase.

- (3) The Fe in the solid base metal reacts with Al preferentially to form Fe_2Al_5 for the heating of the front arc. Some $\text{Fe}_4\text{Al}_{13}$ phase is also formed in the non-equilibrium reaction. With the accumulation of Si in the interface layer, the Fe-Al-Si system is formed. And the $\text{Fe}_3\text{Al}_2\text{Si}_4$ is the Fe-Al-Si system reactant. The Cr in stainless steel diffuses into the weld metal to replace part of Fe and form Fe (Cr)-Al-Si compound.
- (4) The lead wire plays a dominant role in the melting of aluminum side and the interface reaction of steel and aluminum, while the trail wire fills the molten pool, and its arc pressure and droplet impact force increase the stirring effect of the molten pool. Those increase the difficulty of the diffusion of Fe into the liquid molten pool formed by the trail wire. Therefore, the thickness of IMC layer in twin-wire CMT weld brazing is thinner.
- (5) The tension test results show that the fracture occurs at the brazing interface in all joints and the maximum tensile strength of the weld joints is up to 96 MPa, which is about 35% of the strength of the base material.

Funding The authors would like to thank the Science and Technology Planning Project of Guangdong Province (No. 2017A070701026), Guangzhou Science and Technology Project (No. 201807010035; No. 201704030068; No. 201604046026), and Science and Technology Planning Project of Guangdong Academy of Science (No. 2020GDASYL-20200302013; 2017GDASCX-0119; No. 2017GDASCX-01) for their financial support.

References

1. Shah LH, Ishak M (2016) Materials and manufacturing processes review of research progress on aluminum–steel dissimilar welding. *Adv Manuf Process* 29:928–933. <https://doi.org/10.1080/10426914.2014.880461>
2. Agudo L, Eyidi D, Schmaranzer CH, Arenholz E, Jank N, Bruckner J, Pyzalla AR (2007) Intermetallic FeAl₃ phases in a steel/Al-alloy fusion weld. *J Mater Sci* 42:4205–4214. <https://doi.org/10.1007/s10853-006-0644-0>
3. Matysik P, Józwiak S, Czujko T (2015) Characterization of low-symmetry structures from phase equilibrium of Fe-Al system—microstructures and mechanical properties. *Materials* 8:914–931. <https://doi.org/10.3390/ma8030914>
4. Li W, Vairis A, Preuss M, Ma T (2016) Linear and rotary friction welding review. *Int Mater Rev* 61:71–100. <https://doi.org/10.1080/09506608.2015.1109214>
5. DebRoy T, Bhadeshia HKDH (2010) Friction stir welding of dissimilar alloys – a perspective. *Sci Technol Weld Join* 15:266–270. <https://doi.org/10.1179/174329310X12726496072400>
6. Mathieu A, Pontevicci S, Viala J, Cicala E, Mattei S, Grevey D (2006) Laser brazing of a steel/aluminium assembly with hot filler wire (88% Al, 12% Si). *Mater Sci Eng A* 435–436:19–28. <https://doi.org/10.1016/j.msea.2006.07.099>
7. Su Y, Hua X, Wu Y (2014) Influence of alloy elements on microstructure and mechanical property of aluminum–steel lap joint made by gas metal arc welding. *J Mater Process Technol* 214: 750–755. <https://doi.org/10.1016/j.jmatprotec.2013.11.022>
8. Sierra G, Peyre P, Beaume FD, Stuart D, Fras G (2008) Steel to aluminium braze welding by laser process with Al–12Si filler wire. *Sci Technol Weld Join* 13:430–437. <https://doi.org/10.1179/174329308X341852>
9. Song JL, Lin SB, Yang CL, Ma GC, Liu H (2009) Spreading behavior and microstructure characteristics of dissimilar metals TIG welding–brazing of aluminum alloy to stainless steel. *Mater Sci Eng A* 509:31–40. <https://doi.org/10.1016/j.msea.2009.02.036>
10. He H, Wu C, Lin S, Yang C (2019) Pulsed TIG welding–brazing of aluminum–stainless steel with an Al-Cu twin hot wire. *J Mater Eng Perform* 28:1180–1189. <https://doi.org/10.1007/s11665-018-3848-y>
11. He H, Lin S, Yang C, Fan C, Chen Z (2013) Combination effects of Nocolok flux with Ni powder on properties and microstructures of aluminum–stainless steel TIG welding–brazing joint. *J Mater Eng Perform* 22:3315–3323. <https://doi.org/10.1007/s11665-013-0615-y>
12. Shao L, Shi Y, Huang JK, Wu SJ (2015) Effect of joining parameters on microstructure of dissimilar metal joints between aluminum and galvanized steel. *Mater Des* 66:453–458. <https://doi.org/10.1016/j.matdes.2014.06.026>
13. Ye Z, Huang J, Gao W, Zhang Y, Cheng Z, Chen S, Yang J (2017) Microstructure and mechanical properties of 5052 aluminum alloy/mild steel butt joint achieved by MIG-TIG double-sided arc welding–brazing. *Mater Des* 123:69–79. <https://doi.org/10.1016/j.matdes.2017.03.039>
14. Zhang Y, Huang J, Cheng Z, Ye Z, Chi H, Peng L, Chen S (2016) Study on MIG-TIG double-sided arc welding–brazing of aluminum and stainless steel. *Mater Lett* 172:146–148. <https://doi.org/10.1016/j.matlet.2016.02.146>
15. Cao R, Yu G, Chen JH, Wang P-C (2013) Cold metal transfer joining aluminum alloys-to-galvanized mild steel. *J Mater Process Technol* 213:1753–1763. <https://doi.org/10.1016/j.jmatprotec.2013.04.004>
16. Zhang HT, Feng JC, He P, Zhang BB, Chen JM, Wang L (2009) The arc characteristics and metal transfer behaviour of cold metal transfer and its use in joining aluminium to zinc-coated steel. *Mater Sci Eng A* 499:111–113. <https://doi.org/10.1016/j.msea.2007.11.124>
17. Lin SB, Song JL, Yang CL et al (2010) Brazability of dissimilar metals tungsten inert gas butt welding–brazing between aluminum alloy and stainless steel with Al–Cu filler metal. *Mater Design* (1980–2015) 31:2637–2642. <https://doi.org/10.1016/j.matdes.2009.12.005>
18. Stein F, Palm M (2007) Re-determination of transition temperatures in the Fe-Al system by differential thermal analysis. *Int J Mater Res* 98:580–588. <https://doi.org/10.3139/146.101512>
19. Springer H, Kostka A, Payton EJ, Raabe D, Kaysser-Pyzalla A, Eggeler G (2011) On the formation and growth of intermetallic phases during interdiffusion between low-carbon steel and aluminum alloys. *Acta Mater* 59:1586–1600. <https://doi.org/10.1016/j.actamat.2010.11.023>
20. Song JL, Lin SB, Yang CL, Fan CL (2009) Effects of Si additions on intermetallic compound layer of aluminum–steel TIG welding–brazing joint. *J Alloys Compd* 488:217–222. <https://doi.org/10.1016/j.jallcom.2009.08.084>

Publisher's note Springer Nature remains neutral with regard to jurisdictional claims in published maps and institutional affiliations.